

Contents lists available at ScienceDirect

Chemosphere

journal homepage: www.elsevier.com/locate/chemosphere



Ultra-high arsenic adsorption by graphene oxide iron nanohybrid: Removal mechanisms and potential applications



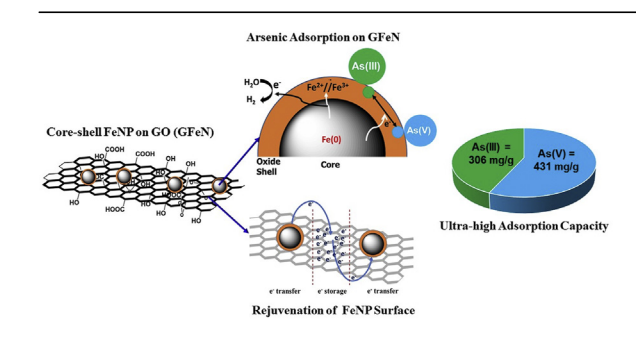
Tonoy K. Das ^a, Tamil S. Sakthivel ^b, Aadithya Jeyaranjan ^b, Sudipta Seal ^{b, c}, Achintya N. Bezbaruah ^{a, *}

- ^a Nanoenvirology Research Group, Department of Civil and Environmental Engineering, North Dakota State University, Fargo, ND, 58105, USA
- ^b Advanced Materials Processing and Analysis Center (AMPAC), Nanoscience and Technology Center (NSTC), Materials Science and Engineering (MSE), University of Central Florida. Orlando. USA
- ^c College of Medicine, University of Central Florida, Orlando, FL, 32826, USA

HIGHLIGHTS

- Graphene oxide iron nanohybrid (GFeN) exhibited rapid arsenic removal kinetics.
- Ultra-high 306 mg As(III) and 431 mg As(V) was adsorbed per gram of GFeN.
- GFeN worked over a wide pH range (3-9) and in the presence of coexisting ions/compounds.
- Arsenic removal mechanisms of include electrostatic attraction and surface complexations.
- Graphene oxide stores electron and transfers them to the iron nanoparticles for rejuvenation.

G R A P H I C A L A B S T R A C T



ARTICLE INFO

Article history:
Received 27 December 2019
Received in revised form
30 March 2020
Accepted 2 April 2020
Available online 8 April 2020

Handling Editor: Y Yeomin Yoon

Keywords: Iron nanohybrid Arsenic Arsenite Arsenate Adsorption Graphene oxide

ABSTRACT

Iron (Fe)-based adsorbents have been promoted for aqueous arsenic adsorption because of their low cost and potential ease of scale-up in production. However, their field application is, so far, limited because of their low Fe use efficiency (i.e., not all available Fe is used), slow adsorption kinetics, and low adsorption capacity. In this study, we synthesized graphene oxide iron nanohybrid (GFeN) by decorating iron/iron oxide (Fe/Fe_xO_y) core-shell structured iron nanoparticles (FeNPs) on the surface of graphene oxide (GO) via a sol-gel process. The deposition of FeNPs on GO for the nanohybrid (GFeN) improves Fe use efficiency and arsenic mobility in the nanohybrid, thereby improving the arsenic removal capacity and kinetics. We achieved removal capacities of 306 mg/g for As(III) and 431 mg/g for As(V) using GFeN. Rapid reduction (>99% in <10 min) of As(III) and As(V) (initial concentration, $C_0 = 100 \,\mu\text{g/L}$) was achieved with the nanohybrid (250 mg/L). There were no significant interferences by the coexisting anions and organic matters at environmentally relevant concentrations. Based on the experimental data, we have proposed that both electrostatic interaction and surface complexation contributed to ultra-high arsenic removal by GFeN. The GO sheets acted as the reservoirs for the electrons released during surface corrosion of the FeNPs and the electrons were transferred back to the FeNPs to rejuvenate the oxidized surface. The rejuvenated FeNP surface layer helped in additional arsenic removal.

© 2020 Elsevier Ltd. All rights reserved.

E-mail address: a.bezbaruah@ndsu.edu (A.N. Bezbaruah).

^{*} Corresponding author.

1 Introduction

Arsenic (As) is predominately a naturally occurring (geogenic) metalloid present in water (Meharg and Zhao, 2012). Inorganic arsenic in both As(III) and As(V) are the most prevalent species in groundwater. The maximum contaminant level (MCL) for total arsenic in drinking water is 10 µg/L (USEPA, 2001; WHO, 2003). Arsenic contamination of drinking water is a major public health concern across the globe and has affected more than 140 million people across 50 countries with Bangladesh, India, Argentina, Canada, Chile, Japan, and Taiwan being most affected (Murcott, 2012; WHO, 2018). About 2.1 million people in the United States who rely on domestic wells for their drinking water are in danger of facing arsenic contamination (>10 μ g/L) (Ayotte et al., 2017). Excess arsenic in drinking water cause several health problems including skin lesions, respiratory problems, neurological complications, and circulatory disorders (Chen et al., 2009). Consumption of water high in arsenic may lead to cancers of skin and internal organs (liver, kidney, lung, and bladder) (WHO, 2018).

While adsorption is the most adopted method for arsenic removal, coagulation, flocculation, precipitation, ion exchange, and membrane filtration are also used. An ideal adsorbent should have high adsorption capacity, affinity for both the inorganic arsenic species (As(III) and As(V)) and should be effective under relevant environmental conditions.

Among several adsorbents, iron (Fe) based adsorbents are very effective and widely used to remove arsenic (Hao et al., 2018). Nanomaterials, mostly nano magnetite (M) and nanoscale zerovalent iron (NZVI) (Bezbaruah et al., 2013; Ling and Zhang, 2014; Tucek et al., 2017; Xu et al., 2019), are effective for arsenic removal because of their very high specific surface area and good adsorption capacity. However, these particles agglomerate easily and get oxidized rapidly (NZVI) (Krajangpan et al., 2012; Stefaniuk et al., 2016). Embedding iron nanoparticles (FeNPs) on sheets of carbonaceous materials enhances aqueous dispersion of the nanoparticles (Ma et al., 2013; Mortazavian et al., 2018), and graphenebased materials are found to be one of the most promising carbonaceous materials for such applications (Wang et al., 2013; Yoon et al., 2016). Graphene oxide (GO) based nanohybrid produced with iron nanoparticles deposited on GO showed improved dispersion behavior in water (Chandra et al., 2010; Huong et al., 2016; Yoon et al., 2016). GO is a 2D carbon sheet with sp² hybridization with a very high specific surface area (320–940 m² g⁻¹) (Gao, 2015; Perreault et al., 2015). GO also contains a large number of hydrophilic groups -OH, - COOH, C=O), and so has good dispersibility in aqueous media (Gao, 2015; Perreault et al., 2015). The functional groups in GO sheet also act as the nucleation sites for nanomaterial formation and facilitate a higher number of nanoparticles to be dispersedly deposited on the GO surface (Wang et al., 2010; Tang et al., 2011). Dispersed deposition of nanoparticles ensures that the surface area of each deposited nanoparticle is available for reaction with the target contaminants. Such GOnanohybrids are reported to be good adsorbents for various contaminants (Wang et al., 2013; Guo et al., 2014).

The use of GO-iron nanohybrids are reported for metal and metalloid removal including arsenic (Luo et al., 2012; Guo et al., 2014; Hoan et al., 2016; Ren et al., 2018). The most reported GO-iron nanohybrid for arsenic removal is GO-Fe₃O₄ (Chandra et al., 2010; Yoon et al., 2016; Liang et al., 2019). There is also limited reporting on the use of GO-Fe⁰ nanohybrid for arsenic removal (Wang et al., 2014). The reported GO-iron nanohybrids (SI, Table A1) have shown limited arsenic removal capacity (6–180 mg/g) and that limits the potential life span of the arsenic removal systems to be fabricated with these nanohybrids. To enhance the removal capacity, an iron-based nanoparticle decorated on GO

surface can potentially be used. GO-Fe nanohybrids offer such an architecture where the nanoparticles are well dispersed (less agglomerated) and, hence, will have enhanced contaminant removal efficiency. The GO layer will mediate electron transfer through initial storage of released electron (due to iron oxidation) and late release of electrons back to the iron nanoparticles. If a coreshell structured iron nanoparticle is used with GO, then the coreshell structure will be protected due to active electron transfer and effective life of the GO-Fe nanohybrid will be extended. For the ease of operation and maintenance, we need a treatment system that can run for a longer period of time before any maintenance intervention is needed. Further, the mechanisms of arsenic removal by these hybrid materials are not well investigated and understood.

In this study, we synthesized a GO iron nanohybrid (GFeN) using a sol-gel process where iron/iron oxide (Fe/Fe $_{\rm X}$ O $_{\rm y}$) nanoparticles were decorated on the surface of GO. The new material was tested for its arsenic removal efficiency at environmentally relevant conditions and its field application potential was evaluated. Based on reaction kinetics, isotherm parameters, and characterization information, we have elucidated on the possible arsenic removal mechanisms. We also investigated the potential role of the GO sheet in arsenic removal by GFeN.

2. Experimental methods

2.1. Materials and supplies

Graphene oxide in water (4 g/L, monolayer content >95%) was obtained from Graphena, (Spain), ferrous sulfate (FeSO₄·7H₂O, >99.5% pure), sodium borohydride (NaBH₄, >97% pure) and other chemicals were reagent grade and purchased from VWR (USA). All chemicals were used as received unless otherwise specified. As(III) and As(V) solutions used in this experiment were prepared using individual 1000 mg/L standard stock solutions (Environmental Express, USA). Deoxygenated deionized (DDI) water was used in this research.

2.2. Material synthesis

GFeN synthesis was done using a sol-gel process (details in SI, Section A2). Briefly, 250 mg of GO was ultrasonicated in 125 mL DDI water for 1 h and transferred into 300 mL round-bottom reaction flask, and the content was purged with N2 gas for 30 min. A freshly prepared FeSO₄·7H₂O solution (2.25 g in 50 mL DDI water) was added, and the mixture was continuously stirred in a magnetic stirrer for 30 min. The pH of the mixture was then adjusted to 6.0–6.1 using 1 M NaOH. The temperature of the mixture was then raised to 60 °C followed by dropwise addition of NaBH₄ solution (0.99 g in 30 mL DDI water) under continuous stirring and N₂ environment, and the mixture was then stirred in the flask for an additional 4 h to allow for the reaction to complete [30]. Black colored precipitates were produced, and the black precipitates were washed with DDI water and ethanol and vacuum dried at 40 °C for 40 h under nitrogen environment. The dried precipitates were ground to get GFeN and the final product was stored in glass vials purged with nitrogen. The yield of GFeN in the process was 650 ± 30 mg which was ~27% (based on total raw materials used). Iron nanoparticles (FeNPs) were also synthesized and stored using the same procedure (as in GFeN) but without the addition of GO and were used in control experiments.

2.3. Characterization

Transmission electron microscopy (TEM) images were obtained using a JEOL JEM-2100 LaB₆ transmission electron microscope (JEOL

USA, Peabody, MA, USA) ran at 200 kV. Raman spectroscopy measurements were conducted on a RM 1000B Micro-Raman Spectrometer (Renishaw, West Dundee, IL, USA) at the Ar-514.5 nm excitation unit. High-Resolution X-ray Photoelectron Spectroscopy (HR-XPS) was performed on a Thermo Fisher ESCALAB 250Xi spectrometer (Thermo Fisher Scientific, Waltham, MA USA) with a monochromated Al K α X-beams (h $\nu=1486.7$ eV). Peak fitting was accomplished by utilizing Avantage XPS program. A Zetasizer Nano ZS (Malvern Panalytical Ltd, Malvern, UK) was used to measure zeta potential. The samples were vacuum degassed at 80 °C for 12 h and then the specific surface area measurements were done using a Quantachrome Nova-e surface area analyzer.

2.4. Batch studies

Amber glass vials (40 mL) fitted with a plastic cap and silicon septum were used as batch reactors. To understand the effects of pH on arsenic removal by GFeN, batch reactors with As(III) or As(V) (30 mL of 5 mg As/L with 10 mg of nanomaterials) were prepared and the initial solution pH was adjusted with 0.1 M HCl or 0.1 M NaOH without any additional buffering and pH adjustment during the experiment. For all other studies an adsorbent (GFeN) dose of 250 mg/L (10 mg in 40 mL) was used in a 60 mL amber glass vial containing different initial As(III) or As(V) concentrations at initial solution pH at 7. The reactors were rotated in a custom-made end-over-end shaker (28 rpm) at room temperature (22 \pm 2 °C, except in the temperature study) for 24 h. The adsorbent was filtered out from the bulk solution using 0.22 μ m syringe filters (VWR, USA) and the filtrate was stored in 1% HNO3 for later arsenic analysis using a

Graphite Furnace Atomic Absorption Spectrophotometer (GF-AAS, PerkinElmer AAS 900H, Waltham, MA, USA). The amount of arsenic adsorbed ($q_{\rm e}$, mg/g) onto the adsorbent was calculated (Eq. (1)). Isotherm and kinetic studies were conducted, and the effects of temperature and interferences by coexisting ions and compounds were investigated (method details in SI).

$$q_e = (C_0 - C_e) \times V_{/m} \tag{1}$$

where, q_e , is the amount of arsenic adsorbed (mg/g) by the adsorbent, C_0 is the initial and C_e is the equilibrium arsenic concentration in the solution (mg/L), V is the volume of bulk solution (L), and m is the mass of the adsorbent (g) used.

2.5. Quality control and statistical analysis

All experiments were conducted in triplicates and the average values are reported here along with the standard deviations. ANOVA analysis was done to determine statistically significant differences in data sets and Tukey's pairwise comparison was used to identify the data that were significantly different.

3. Results and discussion

3.1. Material characterization

TEM micrographs show that the fresh (unused) GO sheets (Fig. 1a) are irregular in shape and a few micrometers in size (\sim 0.51 μ m in the shorter direction and \sim 4.10 μ m in the longer

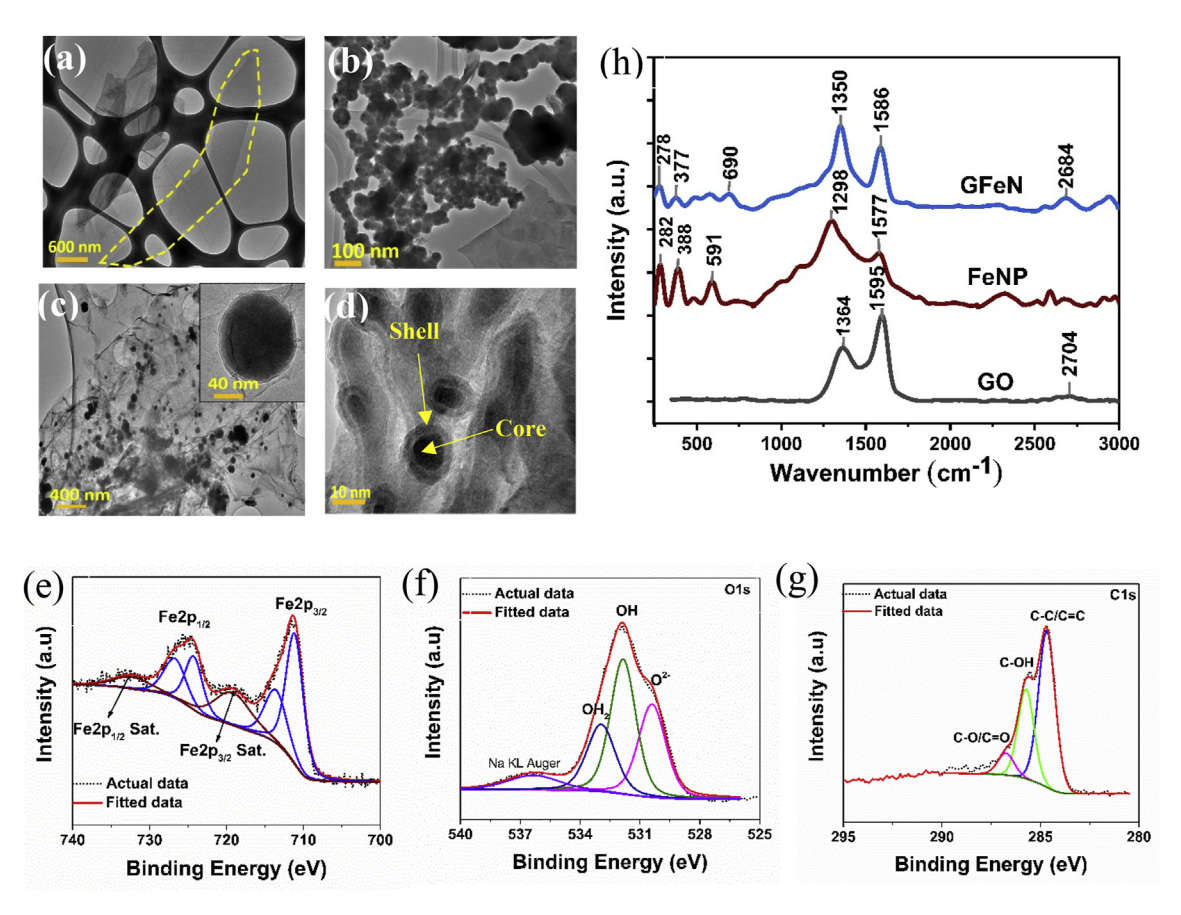


Fig. 1. TEM micrographs (a–d) of (a) a GO sheet (dotted outline, looks irregular in shape and has layered structure), (b) FeNPs synthesized separately (not on GO), and they appear agglomerated, (c) GFeN where nanoparticle are seen dispersed on GO surface (Inset: single FeNP particle on GO), and (d) GFeN where core-shell structured FeNPs and FeNPs trapped between GO layers can be seen). High resolution-XPS spectrum (e–g) obtained from GFeN for (e) Fe 2p, (f) O1s, and (g) C1s. Fe 2p and O1s indicate that oxidized surface of GFeN have both FeOOH and Fe_2O_3/Fe_3O_4 with FeOOH being predominant. (h) Raman spectra for GO, FeNPs, and GFeN. The characteristic D and G peaks confirm the presence GO layer. The shifts in peak locations (D and G) (in GFeN compared to GO) indicate the deposition FeNPs on GO to form GFeN.

direction) and folded in nature. Similar observations were made by others (Wang et al., 2014; Yoon et al., 2016). The bare FeNPs are found to be spherical in shape and clustered together (diameter = 15.3–65.3 nm, n = 31, Fig. 1b). GFeN (Fig. 1c) has nanoparticles decorated on the GO sheets and the particles are well dispersed. The FeNPs decorated on GO (GFeN) have a size distribution of 21.1–88.5 nm (n = 50). Careful observation of the nanohybrid (GFeN) indicates that the nanoparticles are not only deposited on the GO surface but also trapped in between the GO sheets (Fig. 1c–d). The BET specific surface areas of GO was found to be 252.12 m²/g, and it was 88.18 m²/g for FeNPs and 159.62 m²/g for GFeN

XPS analyses of fresh bare FeNPs (Fig. A1a) show the Fe2p core levels with the deconvoluted peaks of Fe $(2p_{3/2})$, Fe $(2p_{1/2})$, and the shake-up satellite peaks. The deconvoluted Fe2p envelop show a small peak of Fe⁰ along with other feature peaks suggesting that the surface consists of a large fraction of iron oxides/iron hydroxide and a relatively small amount of elemental iron (Fe⁰) (Liu et al., 2014). This is in conformity with core-shell structure of FeNPs reported by others (Li and Zhang, 2007; Martin et al., 2008; Liu et al., 2014) and also observed in our HRTEM micrographs (Fig. 1b). This observation was expected as the nanoparticles were prepared in the water where the Fe⁰ and iron oxides are eventually converted to oxyhydroxide on the surface which can be ascribed by a series of chemical reactions (Eqs. (2)–(4)) (Roberts et al., 2004; Liu et al., 2014).

$$4Fe^0 + 3O_2 + 2H_2O \rightarrow 4FeOOH$$
 (2)

$$4Fe_3O_4 + O_2 + 6H_2O \rightarrow 12FeOOH$$
 (3)

$$Fe_2O_3 + H_2O \rightarrow 2FeOOH \tag{4}$$

The Fe2p core level of GFeN (Fig. 1e) shows no elemental iron (Fe⁰) suggesting that the material surface consists mostly of iron oxide/hydroxides in the form of Fe₂O₃, Fe₃O₄, or/and FeOOH. Iron oxide and hydroxide have similar XPS peak positions in this region, and therefore, O1s spectrum (Fig. 1f) is used to determine the existing surface oxygen states. The O1s spectrum contains three prominent peaks that are assigned to O²⁻ (~530 eV), OH (~531.8 eV), and OH₂ (~533.1 eV) (Li and Zhang, 2007). The presence of surface OH species (~68%) and Fe-O (~23%) bonds indicate that the oxidized iron is in the form of FeOOH and that is consistent with other reports (Li and Zhang, 2007; Hao et al., 2014; Liu et al., 2014). Again, the broad peak at ~530 eV suggests the presence of Fe₂O₃ and Fe₃O₄. In the spectrum of C1s core levels (Fig. 1g), the peak at 284.6 eV represents the binding energies of C-C/C=C, the peak at 285.8 eV is for C-OH, and the one at 286.7 eV is for C-O/C=O. The intensity of C-OH is high in GFeN (compared to that in GO shown in Fig. A2b) and that could be due to the presence of high –OH group on the GFeN surface. Based on the XPS results, we can suggest that FeOOH and Fe₂O₃/Fe₃O₄ are the predominant components of the oxidized surface of GFeN.

Raman spectrum of the GO (Fig. 1h) shows two major characteristics peaks, D band peak at 1364 cm⁻¹ and G band peak at 1595 cm⁻¹. The small peak at 2704 cm⁻¹ belongs to 2D band of GO. The FeNPs exhibit a broad peak at 1298 cm⁻¹ and three sharp peaks at 282, 388 and 591 cm⁻¹ suggesting that the surface of the nanoparticle is composed of mixed iron oxide and oxyhydroxide (Nieuwoudt et al., 2011; Liu et al., 2015, 2017). The inference from the Raman data agrees very well with that from our XPS data. The Raman spectra of the nanohybrid (GFeN) shows features of iron oxide and GO which clearly demonstrates the successful deposition of FeNPs on GO. Moreover, the clear shifts of the D and G bands indicate a charge transfer between the FeNP and GO sheet (Ban

et al., 2010; Cong et al., 2012). This charge transfer phenomenon can be beneficial as GO can store the electrons released during iron oxidation (and subsequent arsenic adsorption), and the stored electron can be released back to the FeNP surface to rejuvenate the iron surface. The rejuvenated iron surface can facilitate additional arsenic removal.

3.2. Dispersion behavior

The dispersion behavior of nanomaterials was interpreted based on their Zeta potential (ζ) values (Table A2). GO sheets had a high ζ value ($-48\pm0.33\,$ mV) and, hence, exhibited good dispersion behavior via electrostatic stabilization. The FeNPs lacked electrostatic stabilization with their low ζ value ($11.67\pm0.87\,$ mV) and they agglomerated easily. The nanohybrid (GFeN) had a high ζ ($-22.97\pm0.90\,$ mV) and exhibited very good dispersion behavior in aqueous media (also see SI, Section A6).

3.3. Point-of-zero-charge PZC

The point-of-zero-charge (PZC), at which the pH dependent surface charge is zero, was high for both FeNPs (PZC = 8.40) and GFeN (8.05) (Fig. A3). This indicated that the materials would be able to effectively adsorb aqueous arsenic if the adsorption process is controlled by electrostatic process.

3.4. Arsenic removal

3.4.1. Role of pH on arsenic removal

As(V): Both GFeN and FeNPs removed >90% As(V) ($C_0 = 5 \text{ mg/L}$) over a wide pH range (pH 3–9) with maximum removal (>98%) at pH 5–7 (Fig. 2a). Solution pH affects the speciation of As(V) (Fig. A4), and in aqueous media it is typically present as $H_2AsO_4^-$ at pH 2.2–6.9 and $HAsO_4^{2-}$ at pH 6.9–11.5. Further, H_3AsO_4 is the dominant species at extremely low pH (<2.2), and AsO_4^{3-} dominates at high pH (>11.5) (Yoon et al., 2016).

Below PZC, GFeN and FeNPs were more positively charged and attracted the negatively charged As(V) ($H_2AsO_4^-$ and $HAsO_4^{2-}$). It was expected that with increasing pH the net positive surface charge would decrease and there would be a reduction in arsenic adsorption as we hypothesized the adsorption to be controlled by electrostatic process. However, no significant decrease in As(V) removal (Fig. 2a, removal ~ 95%) was observed in the pH range of 3-9 (Two-way ANOVA, p = 0.05). This indicates that other driving forces besides electrostatic attraction might have helped in the removal of As(V). Similar inferences were also drawn by others (Wang et al., 2014; Wu et al., 2017). Besides electrostatic forces, interactions of arsenic species with iron corrosion products such as FeOOH, Fe₃O₄ and Fe₂O₃ play important roles in arsenic removal at all pH (Wu et al., 2017). As(V) was possibly removed simultaneously through electrostatic attraction and surface complexation with corrosion products, and, for that reason, high removal of As(V) by GFeN and FeNPs was observed over a wide pH range (pH 3-9).

As(III): We tested our new nanohybrid for the removal of As(III) as well. As(III) is present as neutral H_3AsO_3 in aqueous media at pH < 9.2 (Fig. A4). Beyond pH 9.3, H_3AsO_3 dissociates into negatively charged arsenite ions ($H_3AsO_3 \leftrightarrow H_2AsO_3^- + H^+$). The neutral As(III) species was adsorbed onto the Fe-based nanohybrids through surface complexation at pH 3−9, and effective removal (>99%) was achieved (Fig. 2b).

3.4.2. Roles of graphene oxide and iron

We tested the reduced GO (rGO) as the GO sheets used in GFeN synthesis might have been reduced by NaBH₄ used. We investigated the possible adsorption of arsenic using pristine GO and rGO

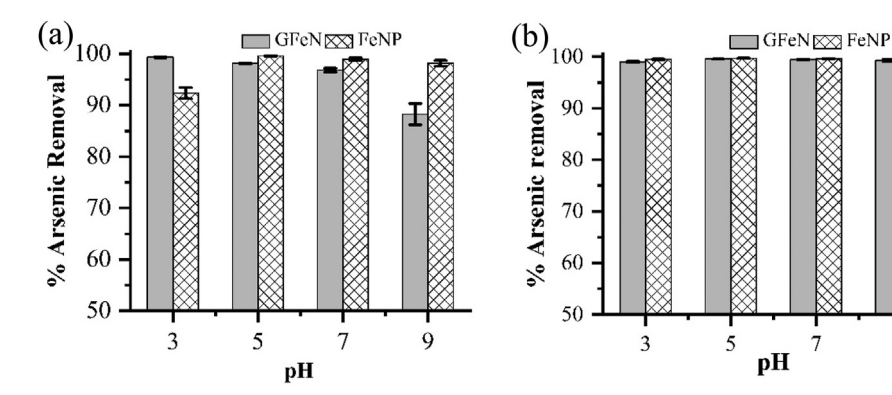


Fig. 2. Arsenic removal at different pH: (a) As(V) and (b) As(III). Initial arsenic concentration $(C_0) = 5 \text{ mg/L}$.

sheets as controls. First, we conducted the experiment with an initial arsenic concentration (C_0) of 5 mg/L but did not record any observable removal by the adsorbents (data not shown). So, we decided to evaluate the GO and rGO sheets at $C_0 = 1 \text{ mg/L}$ (Fig. A5). The pristine GO sheets removed ~12.5% of As(III) and 0.44% of As(V) from 1 mg/L arsenic solution (pH 7). The rGO sheets recorded only 1.8% removal for As(III) and 0.35% for As(V). So, we can infer that our GO sheets in GFeN (present as rGO in the nanohybrid) did not significantly adsorb arsenic but only the FeNPs deposited on the GO sheets did.

In our experiment, we used same mass weight of each adsorbent (GFeN, FeNPs). The Fe content per unit weight of each adsorbent was determined (Table 1, also see Section A4). Even though GFeN had less iron (0.43 g/g) than FeNPs (0.59 g/g), GFeN adsorbed ~38% more As(III) than FeNP across all pH (3-9) (Table 1). In case of As(V), GFeN had ~50% more adsorption capacity than FeNP at pH 3 and ~25% more at pH 9 (Table 1). Higher arsenic removal by GFeN could be due to effective dispersion of FeNPs (reduced agglomeration) in GO layer which ensured improved interactions with arsenic species. Given that GFeN worked as a more efficient adsorbent (than FeNPs), further investigations (subsequent sections) were carried out with GFeN only.

3.4.3. Arsenic removal by GFeN

Kinetic studies: More than 99% removal of arsenic ($C_0 = 5 \text{ mg/L}$) occurred within the first 6 h for As(III) and within 8 h for As(V) (Fig. 3a). The adsorption happened in three distinct stages for both the arsenic species: (1) a rapid removal in the first 60 min (>50%) (Fig. 3a inset), (2) relatively slower removal after 60 min till 6-8 h, and (3) minor (non-significant) removal beyond 6-8 h. The data were fitted onto zero-, first-, and second-order as well as pseudofirst- and pseudo-second-order reaction models (details in SI, section A11). The pseudo-second-order model gave the best fit ($R^2 \sim$ 0.999) for both As(III) and As(V) (Fig. A6, Table A3) which suggests that chemisorption is possibly responsible for the removal of arsenic by GFeN (Wang et al., 2014).

pН

We also measured the Fe in the bulk solution in the 24-h samples. During As(V) removal by GFeN, the total Fe release after 24 h reaction was 0.76 mg/L (0.71% of total Fe in GFeN), and for As(III), the release was 1.03 mg/L (0.95% of total Fe). The results indicate that our nanohybrid was not leaching out any significant amount of iron.

Adsorption isotherm: Langmuir and Freundlich isotherm models were used to understand arsenic sorption behavior by GFeN. Both As(III) and As(V) adsorption data fitted slightly better for Langmuir model ($R^2 = 0.9863$ for As(III) and 0.9818 for As(V)) than the Freundlich ($R^2 = 0.9758$ for As(III) and 0.9586 As(V)) (Fig. 3b-c, Table A5).

Based on the isotherm data, the adsorption capacities of GFeN were found to be 306.10 ± 9.92 mg/g for As(III) and 431.41 ± 25.95 mg/g for As(V) (Table A5). The As(III) and As(V) adsorption capacities of GFeN are very high compared to other GObased nanocomposites so far reported (Table 2). For GFeN, the affinity for sorption (K_1) of As(III) is 0.03846 L/mg and that for As(V) is 0.02314 L/mg, and we used these values to calculated R_L ($R_L = 1/$ $(1 + C_0*K_l$, where C_0 is the initial arsenic concentration) to further elucidate the adsorption process. If $R_L > 1$ then the adsorption process is unfavorable and if $0 < R_L < 1$ then the adsorption is favorable (Hall et al., 1966; Weber and Chakravorti, 1974). For GFeN, arsenic adsorption was found to be favorable for both the arsenic species with $R_L = 0.056-0.997$ for As(III) and 0.072-0.998 for As(V).

3.4.4. Stability of GFeN

A number of batch reactors (amber glass vials) were prepared with 10 mg of GFeN and 40 mL of actual arsenic contaminated groundwater (As(V) \approx 30 µg/L) were prepared and kept in a dark cabinet. Three randomly selected reactors were taken at a

Table 1 Characteristics of iron nanoparticles (FeNPs) and nanohybrid (GFeN) used for arsenic removal in this study.

	= :			-			
Material	Particle Size (nm)	Mean ζ (mV) ^a	Optimal pH ^b	PZC ^c	Fe content g/g	As Removal mg As/g Fe d	
						As(III)	As(V) e
FeNP	15.3-65.3	11.67 ± 0.87	3–9	8.4	0.59	26	32–36
GFeN	21.1-88.5	-22.97 ± 0.90	3-9	8.05	0.43	36	43-49

 $[\]zeta$ = Zeta potential.

pH at which >90% arsenic removal was achieved.

PZC: Point-of-zero-charge.

^d This comparison is done based on arsenic removal by FeNPs and GFeN at $C_0 = 5$ mg/L and the iron content in each nanomaterial was measured for normalization purposes (Sections 3.4.2.)

Adsorption of arsenic decreased as pH increased from 3 to 9.

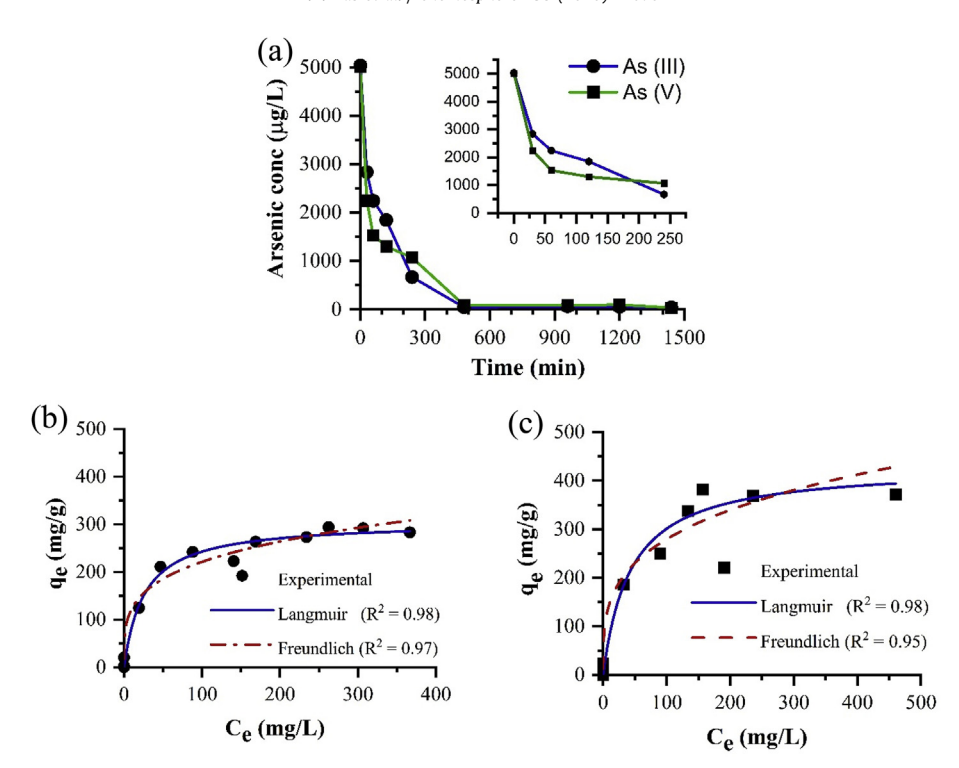


Fig. 3. (a) Arsenic removal by GFeN over time when initial arsenic concentration (C_0) is 5 mg/L (Inset: first 2 h data zoomed in). Langmuir and Freundlich isotherms for: (b) As(III) and (c) As(V). Langmuir fitted better for both the data sets and recorded adsorption capacities of 306.10 \pm 9.92 mg/g for As(III) and 431.41 \pm 25.95 mg/g for As(V). For all experiments: Adsorbent dose = 250 mg/L, and Initial pH = 7.

 Table 2

 Arsenic adsorption capacity for various carbon-based metallic nanohybrids.

Adsorbents	pH ^a	Arsenic concentration range (mg/L)	Adsorbent dose used (g/L)	Adsorption capacity (mg/g)		Source	
				As(III)	As(V)		
Fe ₃ O ₄ -GO	7	0-550	0.1	85	38	Yoon et al. (2016)	
CeO ₂ -GO	_	0.1-200	0.5	185	212	Sakthivel et al. (2017)	
Mg-Al hydroxide/GO	5	0.1-150	0.5	_	180.26	Wen et al. (2013)	
rGO-Fe ₃ O ₄ -TiO ₂	7	3-10	0.2	147.05	_	Benjwal et al. (2015)	
GO-ZrO(OH) ₂	7	2-80	0.5	95.15	84.89	Luo et al. (2013)	
β-FeOOH@GO-COOH	6.5	1-200	1	77.5	45.7	Chen et al. (2015)	
GO-MnFe ₂ O ₄	1-2	10-50	0.2	_	240.3	Huong et al. (2016)	
FeMnO _x /RGO		0.2-7	0.2	22.17	22.05	Zhu et al. (2015)	
Macro-porous magnetic 3D GO hydrogel	~7	0-150	1	25.1	74.2	Liang et al. (2019)	
GNP/Fe-Mg oxide	7	5-90	0.2	_	103.9	La et al. (2017)	
GO-CuFe ₂ O ₄ foam	7.2	5-500	8 L	51.64	124.69	Wu et al. (2018)	
GO-Fe ₂ O ₃	7	0.1-1200	0.8	147	113	Su et al. (2017)	
Fe ₃ O ₄ @CuO-GO	7	3.75-75	0.3	70.36	62.60	Wu et al. (2019)	
GO-lanthanum fluoride	_	2-30	0.8	_	18.52	Lingamdinne et al. (2019)	
Fe ₂ O ₃ nanocubes- porous GO aerogel	_	5-70	0.5	172.27	217.34	Yu et al. (2019)	
GFeN	7	0.1-550	0.25	306.10	431.41	This study	

^a pH at which the experiment was conducted.

predetermined time (0, 1, 5, 18, and 30 d) and spiked with arsenic (with As(V) standard solution) to achieve an arsenic concentration of 450 $\mu g/L$. The set of three reactors in put in the end-over-end shaker (28 rpm) for 12 h and the arsenic concentration was measured in the bulk solution after 12 h to calculate the removal efficiency. The arsenic removal till 5 days remained ~99% and then it slightly decreased to ~93% (18 d) and remained unchanged till 30 d (Fig. A9).

3.4.5. Interferences by co-existing ions and compounds

The ions in groundwater that may potentially interfere with arsenic removal by GFeN include phosphate (PO_4^{3-} , typical

groundwater concentration ~0.32 μ M), bicarbonate (HCO $_3$, ~3 mM), silicate (SiO $_3^2$, ~0.3 mM), nitrate (NO $_3$, <0.16 mM), sulfate (SO $_4^2$, ~1 mM) and compounds like natural organic matters (NOM, <1 mg/L) (Van der Leeden, 1990; Karanfil et al., 2002). The role of ionic strength (typical value 0.001–0.02 mM) on arsenic removal by GFeN was also evaluated. Further, the adsorption efficiency of GFeN was determined when As(III) and As(V) are present together.

 SO_4^{2-} , NO_3^{-} and HCO_3^{-} (0–10 mM) had a negligible effect on the removal of both the arsenic species by GFeN (Fig. 4a–b).

In the presence of low $PO_4^{\frac{2}{3}}$ concentration (0.1 mM), the As(III) removal efficiency decreased from ~99% (0 mM $PO_4^{\frac{2}{3}}$) to ~95% (Fig. 4a), and As(V) removal decreased to ~91% (Fig. 4b). The

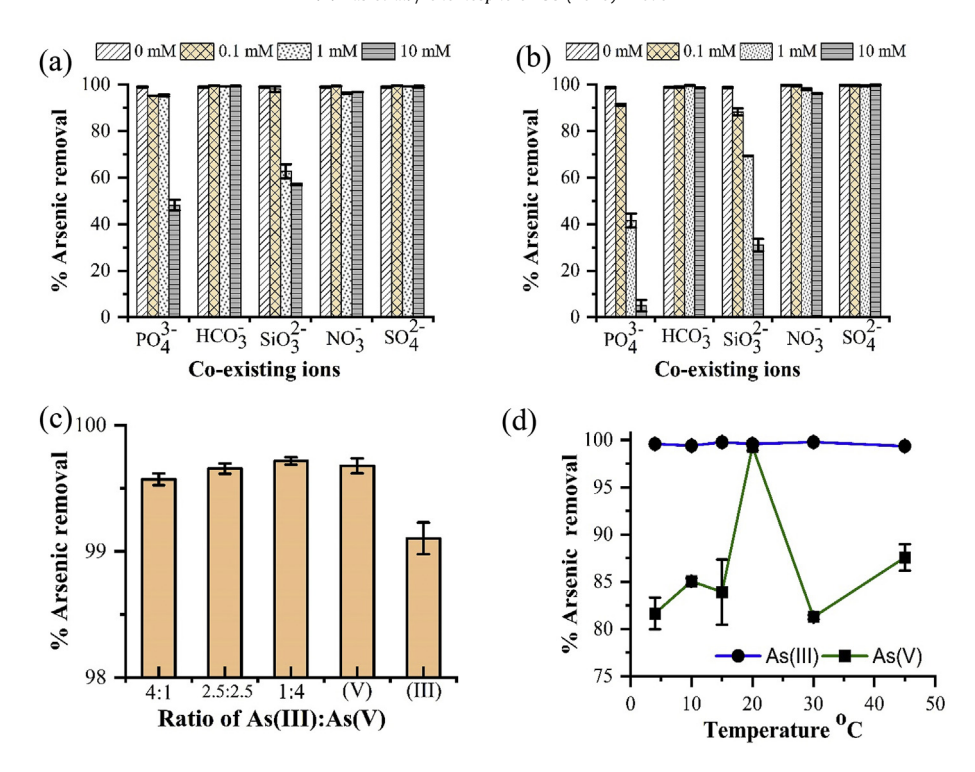


Fig. 4. Arsenic removal by GFeN in the presence of co-existing anions while treating (a) As(III) and (b) As(V), phosphate and silicates ions interfered in arsenic removal but only at above environmental significant concentrations (c) both As(III) and As(V) co-exist (in different mass ratios, (V) and (III) on the x-axis represent 5 mg/L of only As(V) or As(III) and (d) Arsenic removal by GFeN under different temperatures Initial arsenic concentration $(C_0) = 5$ mg/L, Adsorbent dose = 250 mg/L, and Initial pH = 7; for (c) $C_0 = 5$ mg/L total of As(III) and As(V) combined.

removal efficiency further decreased with the increase of PO_4^{3-} concentration (Fig. 4a–b) and the effect was more prominent in As(V) compared to As(III). At 10 mM PO_4^{3-} , As(III) removal was ~48% and As (V) removal was ~5%. It is important to note that PO_4^{3-} concentration in groundwater is typically much below 0.1 mM (WHO, 2004) and, as such, will not affect arsenic removal by GFeN.

In the presence of low SiO_3^{2-} concentration (0.1 mM), the As(III) removal (~97%) was not significantly (p = 0.05) affected relative to the control (~99%) whereas As(V) removal significantly decreased to ~88% (Fig. 4a-b). At 1 mM SiO_3^{2-} concentration, As(III) removal reduced to ~62% and As(V) removal decreased to ~69.2%. When SiO_3^{2-} concentration was increased to 10 mM, the removal efficiencies decreased to ~56% for As(III) and ~31% for As(V). Typical reported concentration of SiO_3^{2-} in groundwater is 0.3 mM, and so we expect some reduction in arsenic removal efficiency when GFeN is used.

There was marginal (6-7%) decrease in arsenic removal when the humic acid concentration was increased from 0 to 10 mg/L (Fig. A8a). In groundwater, organic acid concentration does not typically exceed 1 mg/L (Karanfil et al., 2002) and we did not see any significant decrease in arsenic removal efficiency when the organic acid present was 1 mg/L.

Ionic strength 0–1 M did not affect arsenic adsorption by GFeN (removal >98%) (Fig. A8b). Typical groundwater ionic strength is 0.001–0.02 M (Wallace et al., 2012), and, as such, GFeN is expected to effectively work in any groundwater contaminated with arsenic.

Co-existing arsenic species: To simulate the field situation when As(III) and As(V) are present at the same time, a series of experiments were conducted with an initial combined (As(III) and As(V)) concentration of 5 mg/L with different ratios of the two species. For all combinations, ~99% removal was achieved (Fig. 4c) indicating that GFeN can simultaneously remove both the arsenic species. This is a major advantage with GFeN as most of the reported adsorptive

media can only effectively remove As(V) and pretreatment is called for to oxidize As(III) to As(V). The ability of GFeN for the simultaneous removal of both the species will reduce treatment system complexity and result in cost saving.

3.4.6. Effect of temperature

The temperature (4–45 °C) had significant effects on As(V) removal by GFeN. Optimal As(V) removal (>99%) was achieved at 20 °C, but the removal decreased from 99 to 80–85% when the temperature was either increased or decreased (Fig. 4d). However, As(III) removal was not affected by the temperature variation (4–45 °C) and always remained >99% (Fig. 4d). While mobility of the arsenic species increases with the increase in temperature, electrostatic attraction gets reduced (Wang et al., 2014). Accordingly, we observed reduced As(V) removal at low temperature (low species mobility) as well as high temperature (low electrostatic attraction). However, As(III) removal was not controlled by electrostatic attraction (Section 3.4.1) and, thus, was not affected by temperature change.

3.4.7. Environmental relevance

Arsenic concentration in arsenic contaminated groundwater across the globe is typically around 100 μ g/L. We evaluated the removal of both As(III) and As(V) by the GFeN in the concentration range of 0–140 μ g/L in simulated groundwater (Table A4) and achieved >99% within 30 min in all cases (Fig. 5a). At an initial arsenic concentration of 100 μ g/L, GFeN remediated both As(III) and As(V) to below the MCL (10 μ g/L) within 10 min (Fig. 5b). The arsenic removal data best fitted in a pseudo-second-order model (R² ~ 0.999) for both As(III) and As(V). Effective removal of the arsenic species at these environmentally relevant concentrations in a short time (10–30 min) is promising for field applications.

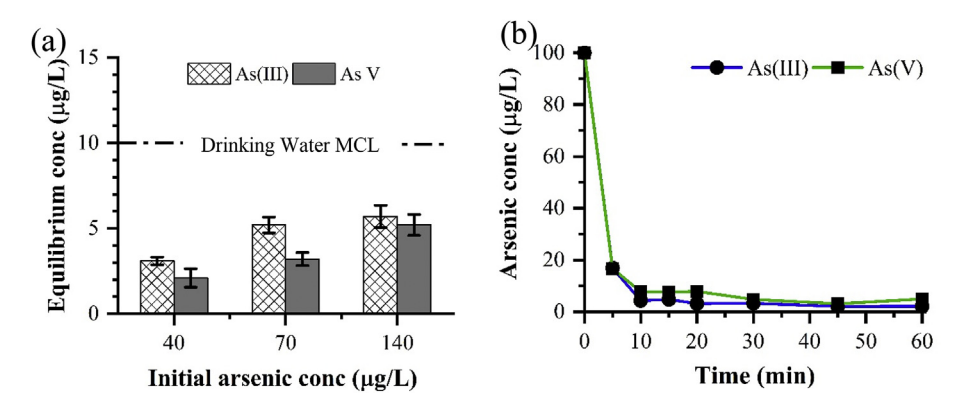


Fig. 5. (a) Arsenic removal at environmental relevant concentrations of $40-140 \mu g/L$ (in simulated groundwater). (b) Arsenic removal by GFeN over time when initial arsenic concentration (C_0) 100 $\mu g/L$. GFeN removed As(III) and As(V) below MCL (10 $\mu g/L$) within 10 min. For all experiments: Adsorbent dose = 250 mg/L, and Initial pH = 7.

3.5. Removal mechanisms

Based on our experimental and characterization data, we are proposing a possible mechanism (Fig. 7) for arsenic removal by the nanohybrid (GFeN). First, the aqueous arsenic ions come in contact with the nanohybrid surface and arsenic flux gradient builds up between the solution and the adsorbent (GFeN) surface. Then the arsenic adsorbs onto the surface of GFeN through electrostatic attraction and surface complexation. Further, the adsorbed arsenic on GFeN surface gets transformed and stabilized within the nanohybrid.

Two types of surfaces are available on the GFeN for arsenic adsorption, the GO sheet and the FeNP surface. However, GO (rGO in GFeN) is not considered as an adsorbent for arsenic in the model as our results indicate that GO sheets do not actively participate in the adsorption process (Fig. A5, rGO in our GFeN removed <2% arsenic, Section 3.4.2).

The XPS spectrum of GFeN after As(V) adsorption shows a strong peak at 45.7 eV (Fig. 6a) which is the characteristic peak for As(V) indicating that there was no change in the oxidation state during the adsorption process. To further understand the possible mechanism, O1s scan of GFeN after As(V) adsorption was analyzed (Fig. 6b) and a significant reduction of OH group (from 68% to 52%) was observed. This result indicates that surface OH species were involved in the formation of inner-sphere monodentate (FeOAsO₂OH) or bidentate ((FeO)₂AsO₂) complex leading to the lowering of OH concentration. Similar results were reported earlier (Eqs. (4) and (5)) (Stachowicz et al., 2008; Hao et al., 2014) and our observations are consistent with that. These equations (Eqs. (5) and (6)) are based on a surface complexation model (aka charge distribution model (CD model)) explained by Stachowicz et al. (2008) (Stachowicz et al., 2008) where ΔZ_0 and ΔZ_1 are the CD model coefficients, and $\Delta Z_0 + \Delta Z_1$ is equal to the charge introduced by the As(V) adsorption process.

$$\equiv FeOH^{-1/2} + 2H^{+} + AsO_{4}^{3-} \rightarrow FeO^{-1/2 + \Delta Z_{0}} AsO_{2}OH^{\Delta Z_{1}} + H_{2}O$$
 (5)

$$2 \equiv FeOH^{-1/2} + 2H^{+} + AsO_{4}^{3-} \rightarrow (FeO)_{2}^{-1/2 + \Delta Z_{0}} AsO_{2}^{\Delta Z_{1}} + 2H_{2}O$$
(6)

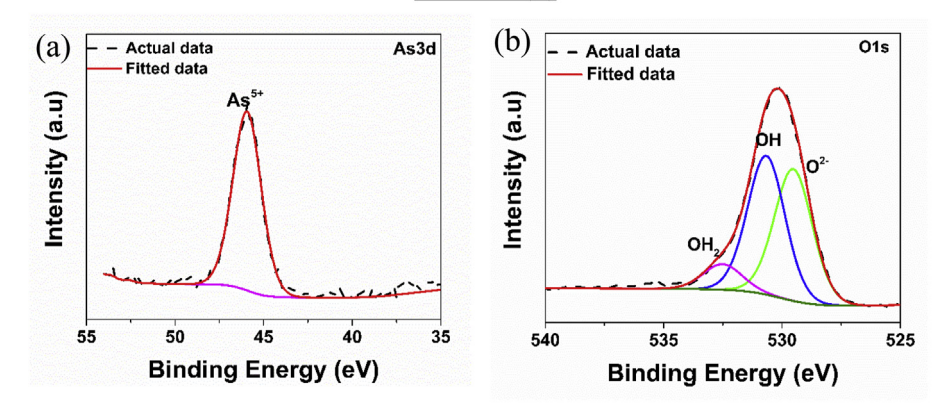
In the case of As(III), the XPS spectrum of arsenic sorbed GFeN indicates that the adsorbed arsenic is in dual oxidation states with As(V) being mostly noticeable on the material's surface and As(III) being relatively less (Fig. 6c). This reveals that As(III) is oxidized to As(V) as it reacts with the iron oxide present on GFeN (Ramos et al.,

2009; Tucek et al., 2017). However, during this oxidation process, elemental iron (Fe⁰) also corrodes simultaneously via the Fenton reaction (Pang et al., 2011) to produce fresh/more iron oxyhydroxide/iron oxide products; in our experiment, this was confirmed by the increase in OH concentration (from 68% to 72%) in the O1s spectrum (Fig. 6d). This suggests that the Fe—O is involved in As(III) adsorption via the formation of inner-sphere surface complex product ((FeO)₂AsOH). In brief, both adsorption and oxidation of As(III) happen simultaneously on GFeN surface. Other reported similar observations during adsorption of arsenic onto iron nanomaterials (Kanel et al., 2006; Farrell and Chaudhary, 2013; Tucek et al., 2017).

 Fe^0 in FeNPs $[Fe/Fe_xO_y]$ deposited on the GO sheet oxidize quickly due to the lower redox potential of the Fe²⁺ and Fe³⁺ couple. During this oxidation, electrons are released by Fe^0 [Fe $^0 \rightarrow$ Fe²⁺ + 2e⁻; Fe²⁺ \rightarrow Fe³⁺ + e⁻], and the GO sheet acts as a reservoir for the released electrons (Lightcap et al., 2010; Wang et al., 2017; Ren et al., 2018). The GO sheet then releases the electrons back to the FeNPs, and iron oxides (on FeNP surface) are converted back to the earlier reduced form ($Fe^{3+} + e^{-} \rightarrow Fe^{2+}$) (Wang et al., 2017). Ren et al. (2018) (Ren et al., 2018) working with hexavalent chromium indicated that there is an active electron transfer process occurring between the decorated iron nanoparticles and the GO sheet, and Wang et al. (2017) (Wang et al., 2017) reported that ion nanoparticles deposited on GO are regenerated by electrons transferred from the graphene oxide sheets during phenol removal. The electron transfer process (from GO to FeNP) helps in maintaining an optimal amount of iron species on the FeNP surface which enhances arsenic adsorption. The major significance of this mechanism is that the overall iron oxidation process is slowed down because of the electron transfer process, and the core Fe⁰ is prevented from getting quickly oxidized (Ren et al., 2018) potentially adding to the active life of the GFeN system.

Additionally, the As(V) \rightarrow As(0) reaction has a potential of 0.499 V while reduction potential of the Fe(0) \rightarrow Fe(II) reaction is -0.477 V, and, thus, As(V) \rightarrow As(0) transformation (SI, Eq. A15 -A23) is thermodynamically favorable (Melitas et al., 2002; Sasaki et al., 2009). The oxide layer on FeNP contains a mixture of amorphous and crystalline iron oxides with the amorphous phase being much larger (2–10 times) than the crystalline phase (Dixit and Hering, 2003; Yan et al., 2012b; Ling and Zhang, 2014; Wu et al., 2017). The porous nature of the amorphous phase, and the lattice disorder and oxygen vacancies in the crystalline phase facilitate faster ionic mobility of arsenic (Kerisit and Rosso, 2005). Both the arsenic species migrate toward the Fe⁰ core (Fig. 7) and gets reduced to an intermetallic phase of As(0) (Yan et al., 2012b; Ling and Zhang, 2014). Intermetallic arsenic species are known to be

GFeN + As(V)



GFeN +As(III)

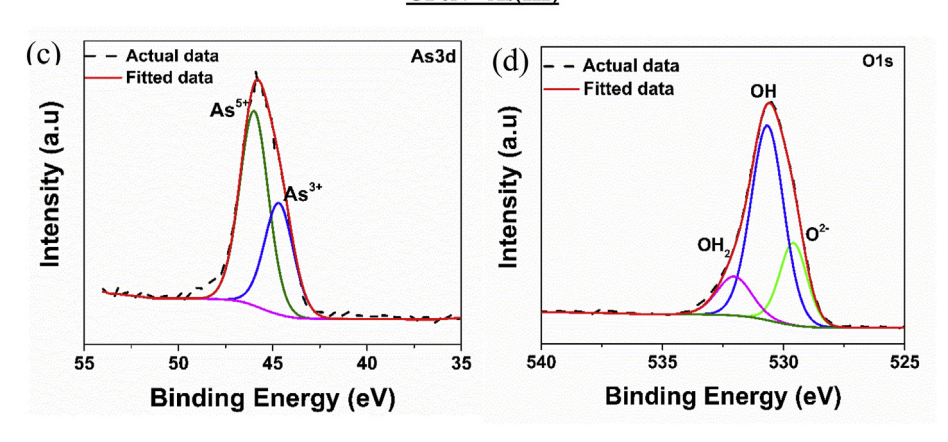


Fig. 6. XPS spectra for GFeN after As(V) adsorption: (a) As3d and (b) O1s; and XPS spectra for GFeN after As(III) adsorption: (c) As3d and (d) O1s.

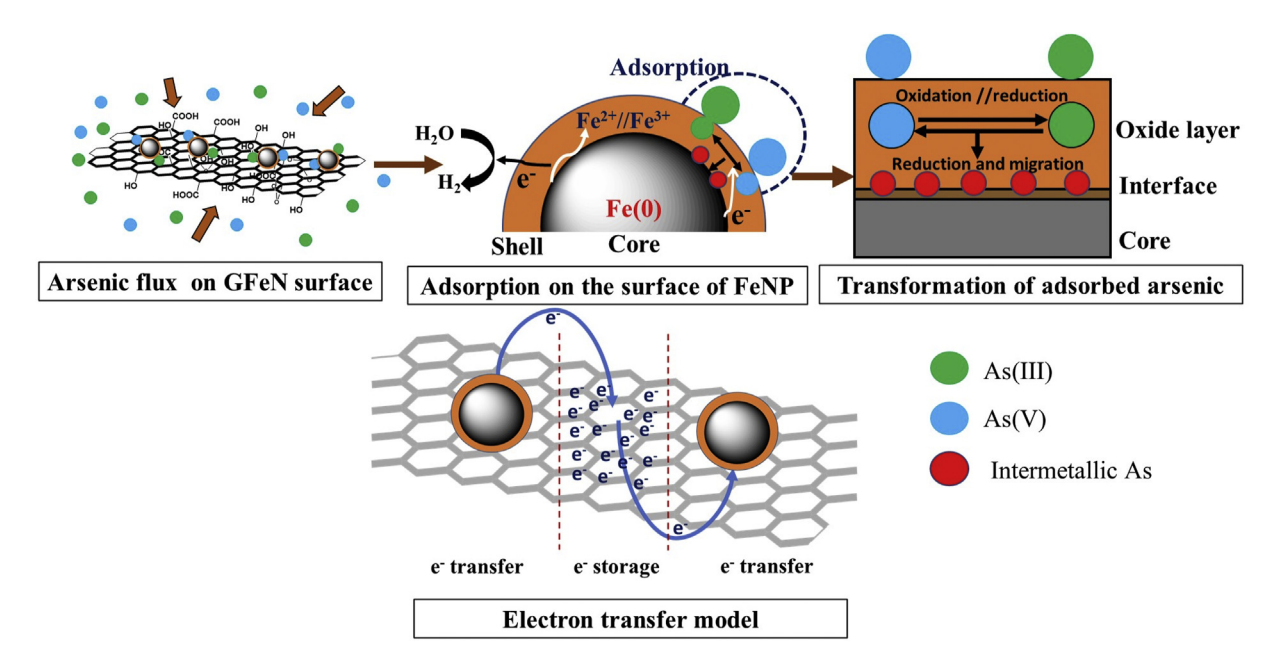


Fig. 7. Top: The possible mechanism for arsenic removal by GFeN. The proposed mechanism involves arsenic flux built-up at the solution-adsorbent interface, followed by adsorption onto the iron nanoparticles (FeNPs) present on GFeN. Simultaneous oxidation and reduction of adsorbed arsenic occur and the reduced arsenic moves to the core of the FeNPs. Bottom: The graphene oxide (GO) sheet acts as the reservoir for electrons (e⁻) released during iron oxidation and the stored electrons are used by the oxide layer (on FeNPs) to rejuvenate itself for further adsorption of arsenic.

more stable than other species (Yan et al., 2012a; Tucek et al., 2017) and that adds to the robustness of the adsorbent (GFeN).

4. Practical significance

The relative high arsenic removal capacity of GFeN (>300 mg As/ g for both the species) and rapid reaction kinetics are very significant for possible field applications of the nanohybrid. Assuming that a typical four-member family needs a minimum of 20 L of drinking water per day, the amount of GFeN needed to treat arsenic contaminated water to meet daily water demand will be 10 g per year (detailed calculations in Section A18, Table A6). It is important to note that this number is calculated assuming only 25% efficiency in arsenic adsorption by GFeN (25% of 300 mg/g = 75 mg As per g of GFeN), a raw water arsenic concentration of 100 µg/L (typical value), and a finished water arsenic concentration of 0 μg/L (MCL Goal, (USEPA, 2019)). If a point-of-use (POU) treatment system is fabricated with 100 g of GFeN, then it is expected to work for ~10 years. Additionally, such systems can be scaled up for community water treatment. This is significant because such a treatment unit will reduce the need for frequent monitoring of the system and water quality. Monitoring water quality is always a challenge in rural and remote communities. Moreover, it will reduce the volume of hazardous waste generated and the frequency of such generation.

5. Conclusions

In this paper, we have reported an easy to adopt synthesis process for graphene oxide-iron nanohybrid (GFeN). GFeN exhibits very high adsorption capacities for As(V) (431 mg/g) and As(III) (306 mg/g) compared to other available nanohybrid sorbents (reported adsorption capacities of 12-240 mg/g, Table 2). At environmentally relevant arsenic concentrations (up to 140 µg/L), GFeN could bring down the effluent arsenic concentrations to below the MCL (10 μ g/L) within 10 min. The adsorbent works for both the species of arsenic even when they were present simultaneously. GFeN nanohybrid removes >90% arsenic even in the presence of potential competing anions (SO_4^{2-} , NO_3^{-} , HCO_3^{-} , PO_4^{3-} , SiO_3^{2-}) and organic matters (organic acid) at environmentally relevant concentrations. Arsenic removal by GFeN is not controlled by electrostatic forces alone but surface complexation played a major role to make it effective across a wide pH range (pH 3-9). Iron nanoparticles (FeNPs) were well dispersed on the graphene oxide (GO) sheets and thus most of the reactive surfaces on the nanoparticles were available for arsenic removal. The GO sheet also played an important role by acting as the reservoir for the released electrons during the oxidation of Fe⁰ present in GFeN and then transferring the electrons back to the nanoparticle (FeNP) surface to rejuvenate the adsorptive oxide layer. We also report a comprehensive mechanism to explain the unique arsenic adsorption behavior of the nanohybrid (GFeN). Interfacial (water and GFeN) exchange of arsenic leads to adsorption through electrostatic attraction and surface complexation, and the adsorbed arsenic then gets transformed and stabilizes in the nanohybrid. The ultra-high adsorption capacity (>300 mg/g for either arsenic species) along with quick reaction kinetics and effectiveness under different environmental conditions make GFeN an ideal candidate for potential use in aqueous arsenic remediation. Our calculations indicate that a point-of-use treatment unit with 100 g of GFeN can potentially supply arsenic free drinking water for ~10 years without much operation and maintenance needs.

Declaration of competing interest

The authors declare that they have no known competing financial interests or personal relationships that could have appeared to influence the work reported in this paper.

CRediT authorship contribution statement

Tonoy K. Das: Conceptualization, Methodology, Data curation, Formal analysis, Visualization, Writing - original draft, Investigation. **Tamil S. Sakthivel:** Visualization, Formal analysis, Writing - original draft. **Aadithya Jeyaranjan:** Data curation, Formal analysis. **Sudipta Seal:** Supervision, Resources, Writing - review & editing, Funding acquisition. **Achintya N. Bezbaruah:** Supervision, Resources, Validation, Writing - review & editing, Project administration, Funding acquisition.

Acknowledgments

This work was funded by National Science Foundation (NSF Grant# CBET- 1707093, PI: Bezbaruah), USGS-North Dakota Water Resources Research Institute, and North Dakota State University (Grand Challenges Initiative). Tonoy Das received funding (fellowships) through NS-ICAR-IF from Indian Council of Agriculture Research and North Dakota Water Resources Research Institute (NDWRRI). Electron microscopy was done at the NDSU Core Laboratory (NSF Grant# CMMI-0821655). Sudipta Seal acknowledges the NSF MRI grant for XPS (NSF Grant# ECCS-1726636).

Appendix A. Supplementary data

Supplementary data to this article can be found online at https://doi.org/10.1016/j.chemosphere.2020.126702.

References

- Ayotte, J.D., Medalie, L., Qi, S.L., Backer, L.C., Nolan, B.T., 2017. Estimating the high-arsenic domestic-well population in the conterminous United States. Environ. Sci. Technol. 51, 12443—12454.
- Ban, C.M., Wu, Z.C., Gillaspie, D.T., Chen, L., Yan, Y.F., Blackburn, J.L., Dillon, A.C., 2010. Nanostructured Fe₃O₄/SWNT electrode: binder-free and high-rate Li-ion anode. Adv. Mater. 22, E145—E149.
- Benjwal, P., Kumar, M., Chamoli, P., Kar, K.K., 2015. Enhanced photocatalytic degradation of methylene blue and adsorption of arsenic(III) by reduced graphene oxide (rGO)-metal oxide (TiO2/Fe3O4) based nanocomposites. RSC Adv. 5, 73249—73260.
- Bezbaruah, A.N., Kalita, H., Almeelbi, T., Capecchi, C.L., Jacob, D.L., Ugrinov, A.G., Payne, S.A., 2013. Ca-alginate-entrapped nanoscale iron: arsenic treatability and mechanism studies. J. Nanoparticle Res. 16 (1), 2175.
- Chandra, V., Park, J., Chun, Y., Lee, J.W., Hwang, I.-C., Kim, K.S., 2010. Water-dispersible magnetite-reduced graphene oxide composites for arsenic removal. ACS Nano 4, 3979—3986.
- Chen, M.L., Sun, Y., Huo, C.B., Liu, C., Wang, J.H., 2015. Akaganeite decorated graphene oxide composite for arsenic adsorption/removal and its proconcentration at ultra-trace level. Chemosphere 130, 52–58.
- Chen, Y., Parvez, F., Gamble, M., Islam, T., Ahmed, A., Argos, M., Graziano, J.H., Ahsan, H., 2009. Arsenic exposure at low-to-moderate levels and skin lesions, arsenic metabolism, neurological functions, and biomarkers for respiratory and cardiovascular diseases: review of recent findings from the Health Effects of Arsenic Longitudinal Study (HEALS) in Bangladesh. Toxicol. Appl. Pharmacol. 239, 184–192.
- Cong, H.P., Ren, X.C., Wang, P., Yu, S.H., 2012. Macroscopic multifunctional graphene-based hydrogels and aerogels by a metal ion induced self-assembly process. ACS Nano 6, 2693—2703.
- Dixit, S., Hering, J.G., 2003. Comparison of arsenic (V) and arsenic (III) sorption onto iron oxide minerals: implications for arsenic mobility. Environ. Sci. Technol. 37, 4182–4189.
- Farrell, J., Chaudhary, B.K., 2013. Understanding arsenate reaction kinetics with ferric hydroxides. Environ. Sci. Technol. 47, 8342–8347.
- Gao, W., 2015. The Chemistry of Graphene Oxide. Graphene Oxide. Springer, pp. 61–95.
- Guo, X.Y., Du, B., Wei, Q., Yang, J., Hu, L.H., Yan, L.G., Xu, W.Y., 2014. Synthesis of amino functionalized magnetic graphenes composite material and its application to remove Cr(VI), Pb(II), Hg(II), Cd(II) and Ni(II) from contaminated water.

- J. Hazard Mater. 278, 211-220.
- Hall, K.R., Eagleton, L.C., Acrivos, A., Vermeulen, T., 1966. Pore and solid-diffusion kinetics in field-bed adsorption under constant-pattern conditions. Ind. Eng. Chem. Fundam. 5, 212-223.
- Hao, L., Ouyang, T., Lai, L., Liu, Y.X., Chen, S., Hu, H., Chang, C.T., Wang, J.-J., 2014. Temperature effects on arsenate adsorption onto goethite and its preliminary application to arsenate removal from simulative geothermal water. RSC Adv. 4, 51984-51990.
- Hao, L.L., Liu, M.Z., Wang, N.N., Li, G.J., 2018. A critical review on arsenic removal from water using iron-based adsorbents. RSC Adv. 8, 39545-39560.
- Hoan, N.T.V., Thu, N.T.A., Van Duc, H., Cuong, N.D., Khieu, D.O., Vo, V., 2016, Fe₃O₄/ Reduced graphene oxide nanocomposite: synthesis and its application for toxic metal ion removal. J. Chem. 10.
- Huong, P.T.L., Huy, L.T., Phan, V.N., Huy, T.Q., Nam, M.H., Lam, V.D., Le, A.T., 2016. Application of graphene oxide-MnFe₂O₄ magnetic nanohybrids as magnetically separable adsorbent for highly efficient removal of arsenic from water. J. Electron. Mater. 45, 2372–2380.
- Kanel, S.R., Greneche, J.M., Choi, H., 2006. Arsenic (V) removal from groundwater using nano scale zero-valent iron as a colloidal reactive barrier material. Environ. Sci. Technol. 40, 2045-2050.
- Karanfil, T., Schlautman, M.A., Erdogan, I., 2002. Survey of DOC and UV measurement practices with implications for SUVA determination. J. AWWA (Am. Water Works Assoc.) 94, 68-80.
- Kerisit, S., Rosso, K.M., 2005. Charge transfer in FeO: a combined molecular-
- dynamics and ab initio study. J. Chem. Phys. 123 (22), 224712. Krajangpan, S., Kalita, H., Chisholm, B.J., Bezbaruah, A.N., 2012. Iron nanoparticles coated with amphiphilic polysiloxane graft copolymers: dispersibility and contaminant treatability. Environ. Sci. Technol. 46, 10130-10136.
- La, D.D., Patwari, J.M., Jones, L.A., Antolasic, F., Bhosale, S.V., 2017. Fabrication of a GNP/Fe-Mg binary oxide composite for effective removal of arsenic from aqueous solution. ACS Omega 2, 218-226.
- Li, X.O., Zhang, W.X., 2007. Sequestration of metal cations with zerovalent iron nanoparticles a study with high resolution X-ray photoelectron spectroscopy (HR-XPS). J. Phys. Chem. C 111, 6939-6946.
- Liang, J.J., He, B.H., Li, P., Yu, J., Zhao, X.L., Wu, H.Y., Li, J., Sun, Y.B., Fan, Q.H., 2019. Facile construction of 3D magnetic graphene oxide hydrogel via incorporating assembly and chemical bubble and its application in arsenic remediation. Chem. Eng. J. 358, 552-563.
- Lightcap, I.V., Kosel, T.H., Kamat, P.V., 2010. Anchoring semiconductor and metal nanoparticles on a two-dimensional catalyst mat. Storing and shuttling electrons with reduced graphene oxide. Nano Lett. 10, 577-583.
- Ling, L., Zhang, W.X., 2014. Sequestration of arsenate in zero-valent iron nanoparticles: visualization of intraparticle reactions at angstrom resolution. Environ. Sci. Technol. Lett. 1, 305-309.
- Lingamdinne, L.P., Koduru, J.R., Chang, Y.Y., Kang, S.H., Yang, J.K., 2019. Facile synthesis of flowered mesoporous graphene oxide-lanthanum fluoride nanocomposite for adsorptive removal of arsenic. J. Mol. Liq. 279, 32-42.
- Liu, A., Liu, J., Han, J., Zhang, W.X., 2017. Evolution of nanoscale zero-valent iron (nZVI) in water: microscopic and spectroscopic evidence on the formation of nano- and micro-structured iron oxides. J. Hazard Mater. 322, 129-135.
- Liu, A., Liu, J., Pan, B., Zhang, W.X., 2014. Formation of lepidocrocite (γ-FeOOH) from oxidation of nanoscale zero-valent iron (nZVI) in oxygenated water. RSC Adv. 4, 57377-57382.
- Liu, A.R., Liu, J., Zhang, W.X., 2015. Transformation and composition evolution of nanoscale zero valent iron (nZVI) synthesized by borohydride reduction in static water. Chemosphere 119, 1068-1074.
- Luo, X., Wang, C., Luo, S., Dong, R., Tu, X., Zeng, G., 2012. Adsorption of as (III) and as V) from water using magnetite Fe3O4-reduced graphite oxide-MnO2 nanocomposites. Chem. Eng. J. 187, 45-52.
- Luo, X.B., Wang, C.C., Wang, L.C., Deng, F., Luo, S.L., Tu, X.M., Au, C.T., 2013. Nanocomposites of graphene oxide-hydrated zirconium oxide for simultaneous removal of As(III) and As(V) from water. Chem. Eng. J. 220, 98-106.
- Ma, J., Zhu, Z., Chen, B., Yang, M., Zhou, H., Li, C., Yu, F., Chen, J., 2013. One-pot, largescale synthesis of magnetic activated carbon nanotubes and their applications for arsenic removal. J. Mater. Chem. 1, 4662-4666.
- Martin, J.E., Herzing, A.A., Yan, W.L., Li, X.Q., Koel, B.E., Kiely, C.J., Zhang, W.X., 2008. Determination of the oxide layer thickness in core-shell zerovalent iron nanoparticles. Langmuir 24, 4329-4334.
- Meharg, A.A., Zhao, F.J., 2012. Arsenic & Rice. Springer Science & Business Media. Melitas, N., Wang, J.P., Conklin, M., O'Day, P., Farrell, J., 2002. Understanding soluble arsenate removal kinetics by zerovalent iron media. Environ. Sci. Technol. 36, 2074-2081.
- Mortazavian, S., An, H., Chun, D., Moon, J., 2018. Activated carbon impregnated by zero-valent iron nanoparticles (AC/nZVI) optimized for simultaneous adsorption and reduction of aqueous hexavalent chromium: material characterizations and kinetic studies. Chem. Eng. J. 353, 781-795.
- Murcott, S., 2012. Arsenic Contamination in the World. IWA publishing.
- Nieuwoudt, M.K., Comins, J.D., Cukrowski, I., 2011. The growth of the passive film on iron in 0.05 M NaOH studied in situ by Raman micro-spectroscopy and electrochemical polarisation. Part I: near-resonance enhancement of the Raman spectra of iron oxide and oxyhydroxide compounds. J. Raman Spectrosc. 42, 1335-1339.
- Pang, S.Y., Jiang, J., Ma, J., 2011. Response to comment on "oxidation of sulfoxides and arsenic(III) in corrosion of nanoscale zero valent iron by oxygen; evidence against ferryl ions (Fe(IV)) as active intermediates in Fenton reaction. Environ.

- Sci. Technol. 45, 3179-3180.
- Perreault, F., De Faria, A.F., Elimelech, M., 2015. Environmental applications of graphene-based nanomaterials. Chem. Soc. Rev. 44, 5861-5896.
- Ramos, M.A.V., Yan, W., Li, X.O., Koel, B.E., Zhang, W.X., 2009. Simultaneous oxidation and reduction of arsenic by zero-valent iron nanoparticles: understanding the significance of the core-shell structure. J. Phys. Chem. C 113, 14591-14594.
- Ren, L.M., Dong, J., Chi, Z.F., Huang, H.Z., 2018. Reduced graphene oxide-nano zero value iron (rGO-nZVI) micro-electrolysis accelerating Cr(VI) removal in aquifer. J. Environ. Sci. 73, 96–106.
- Roberts, L.C., Hug, S.I., Ruettimann, T., Billah, M., Khan, A.W., Rahman, M.T., 2004. Arsenic removal with iron(II) and iron(III) waters with high silicate and phosphate concentrations. Environ. Sci. Technol. 38, 307-315.
- Sakthivel, T.S., Das, S., Pratt, C.J., Seal, S., 2017. One-pot synthesis of a ceria-graphene oxide composite for the efficient removal of arsenic species. Nanoscale 9 (10), 3367-3374.
- Sasaki, K., Nakano, H., Wilopo, W., Miura, Y., Hirajima, T., 2009. Sorption and speciation of arsenic by zero-valent iron, Colloid, Surface, Physicochem, Eng. Aspect. 347, 8-17.
- Stachowicz, M., Hiemstra, T., van Riemsdijk, W.H., 2008. Multi-competitive interaction of as (III) and as (V) oxyanions with Ca^{2+} , Mg^{2+} , PO^{3-} 4, and CO^{2-} 3 ions on goethite. J. Colloid Interface Sci. 320, 400–414.
- Stefaniuk, M., Oleszczuk, P., Ok, Y.S., 2016. Review on nano zerovalent iron (nZVI): from synthesis to environmental applications. Chem. Eng. J. 287, 618–632.
- Su, H., Ye, Z.B., Hmidi, N., 2017. High-performance iron oxide-graphene oxide nanocomposite adsorbents for arsenic removal, Colloid, Surface, Physicochem. Eng. Aspect. 522, 161-172.
- Tang, X.Z., Cao, Z., Zhang, H.B., Liu, J., Yu, Z.Z., 2011. Growth of silver nanocrystals on graphene by simultaneous reduction of graphene oxide and silver ions with a rapid and efficient one-step approach. Chem. Commun. 47, 3084-3086.
- Tucek, J., Prucek, R., Kolarik, J., Zoppellaro, G., Petr, M., Filip, J., Sharma, V.K., Zboril, R., 2017. Zero-valent iron nanoparticles reduce arsenites and arsenates to as(0) firmly embedded in core-shell superstructure: challenging strategy of arsenic treatment under anoxic conditions. ACS Sustain. Chem. Eng. 5, 3027-3038
- United States Environmental Protection Agency (USEPA), 2019. National Primary Drinking Water Regulations. Available at: (Access date December 2, 2019). https://www.epa.gov/ground-water-and-drinking-water/national-primarydrinking-water-regulations.
- United States Environmental Protection Agency (USEPA), 2001. National primary drinking water regulations; arsenic and clarifications to compliance and new source contaminants monitoring. Fed. Regist. 66, 6975-7066.
- Van der Leeden, F., 1990. The Water Encyclopedia. CRC Press.
- Wallace, S.H., Shaw, S., Morris, K., Small, J.S., Fuller, A.J., Burke, I.T., 2012. Effect of groundwater pH and ionic strength on strontium sorption in aquifer sediments: implications for Sr-90 mobility at contaminated nuclear sites. Appl. Geochem. 27, 1482-1491.
- Wang, C., Luo, H.J., Zhang, Z.L., Wu, Y., Zhang, J., Chen, S.W., 2014. Removal of As(III) and As(V) from aqueous solutions using nanoscale zero valent iron-reduced graphite oxide modified composites. J. Hazard Mater. 268, 124-131.
- Wang, H., Robinson, J.T., Diankov, G., Dai, H., 2010. Nanocrystal growth on graphene with various degrees of oxidation. J. Am. Chem. Soc. 132, 3270-3271.
- Wang, P.L., Zhou, X., Zhang, Y.G., Yang, L.P., Zhi, K.K., Wang, L.L., Zhang, L.T., Guo, X.F., 2017. Unveiling the mechanism of electron transfer facilitated regeneration of active Fe²⁺ by nano-dispersed iron/graphene catalyst for phenol removal. RSC Adv. 7, 26983-26991.
- Wang, S.B., Sun, H.Q., Ang, H.M., Tade, M.O., 2013. Adsorptive remediation of environmental pollutants using novel graphene-based nanomaterials. Chem. Eng. J. 226, 336–347.
- Weber, T.W., Chakravorti, R.K., 1974. Pore and solid diffusion models for fixed-bed adsorbers. AIChE J. 20, 228-238.
- Wen, T., Wu, X.L., Tan, X.L., Wang, X.K., Xu, A.W., 2013. One-Pot synthesis of waterswellable Mg-Al layered double hydroxides and graphene oxide nanocomposites for efficient removal of as(V) from aqueous solutions. ACS Appl. Mater. Interfaces 5, 3304–3311.
- World Health Organization (WHO), 2003. Arsenic in Drinking-Water: Background Document for Development of WHO Guidelines for Drinking-Water Quality. WHO/SDE/WSH. /03.04/75.
- World Health Organization (WHO), 2004. Guidelines for Drinking-Water Quality. World Health Organization.
- World Health Organization (WHO), 2018. Arsenic fact sheet. Available at: https:// www.who.int/news-room/fact-sheets/detail/arsenic. (Accessed 23 November
- Wu, C., Tu, J.W., Liu, W.Z., Zhang, J., Chu, S.Q., Lu, G.N., Lin, Z., Dang, Z., 2017. The double influence mechanism of pH on arsenic removal by nano zero valent iron: electrostatic interactions and the corrosion of Fe⁰. Environmental Science-Nano 4, 1544-1552.
- Wu, K., Jing, C.Y., Zhang, J., Liu, T., Yang, S.J., Wang, W.D., 2019. Magnetic Fe₃O₄@CuO nanocomposite assembled on graphene oxide sheets for the enhanced removal of arsenic(III/V) from water. Appl. Surf. Sci. 466, 746-756.
- Wu, L.K., Wu, H., Zhang, H.B., Cao, H.Z., Hou, G.Y., Tang, Y.P., Zheng, G.Q., 2018. Graphene oxide/CuFe₂O₄ foam as an efficient absorbent for arsenic removal from water. Chem. Eng. J. 334, 1808–1819. Xu, L., Yan, K., Mao, Y., Wu, D., 2019. Enhancing the dioxygen activation for arsenic
- removal by Cu⁰ nano-shell-decorated nZVI: synergistic effects and mechanisms.

Chem. Eng. J. 123295.

- Yan, W., Vasic, R., Frenkel, A.I., Koel, B.E., 2012a. Intraparticle reduction of arsenite (as(III)) by nanoscale zerovalent iron (nZVI) investigated with in situ X-ray absorption spectroscopy. Environ. Sci. Technol. 46, 7018–7026.
- Yan, W.L., Ramos, M.A.V., Koel, B.E., Zhang, W.X., 2012b. As(III) sequestration by iron nanoparticles: study of solid-phase redox transformations with X-ray photo-electron spectroscopy. I. Phys. Chem. C 116, 5303—5311.
- electron spectroscopy. J. Phys. Chem. C 116, 5303—5311.

 Yoon, Y., Park, W.K., Hwang, T.M., Yoon, D.H., Yang, W.S., Kang, J.W., 2016.

 Comparative evaluation of magnetite-graphene oxide and magnetite-reduced
- graphene oxide composite for As(III) and As(V) removal. J. Hazard Mater. 304, 196–204
- Yu, X.W., Wei, Y.F., Liu, C.B., Ma, J.H., Liu, H., Wei, S.D., Deng, W., Xiang, J.N., Luo, S.L., 2019. Ultrafast and deep removal of arsenic in high-concentration wastewater: a superior bulk adsorbent of porous Fe₂O₃ nanocubes-impregnated graphene aerogel. Chemosphere 222, 258–266.
- Zhu, J., Lou, Z.M., Liu, Y., Fu, R.Q., Baig, S.A., Xu, X.H., 2015. Adsorption behavior and removal mechanism of arsenic on graphene modified by iron-manganese binary oxide (FeMnOx/RGO) from aqueous solutions. RSC Adv. 5, 67951–67961.